Electronic Supplementary Material (ESI) for Journal of Materials Chemistry A.

Supporting Information

Boosting supercapacitor and capacitive deionization performance of hierarchically porous carbon by polar surface and structural engineering

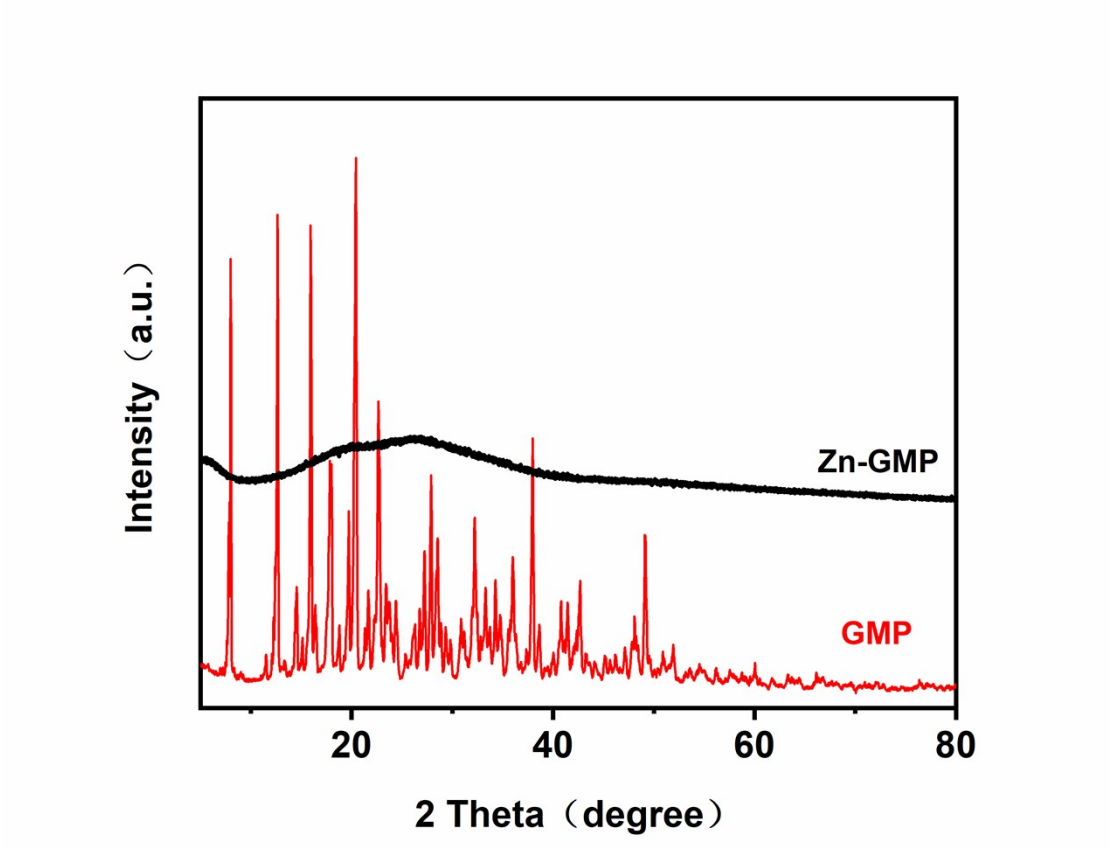

Figure S1. XRD patterns of GMP and Zn-GMP.

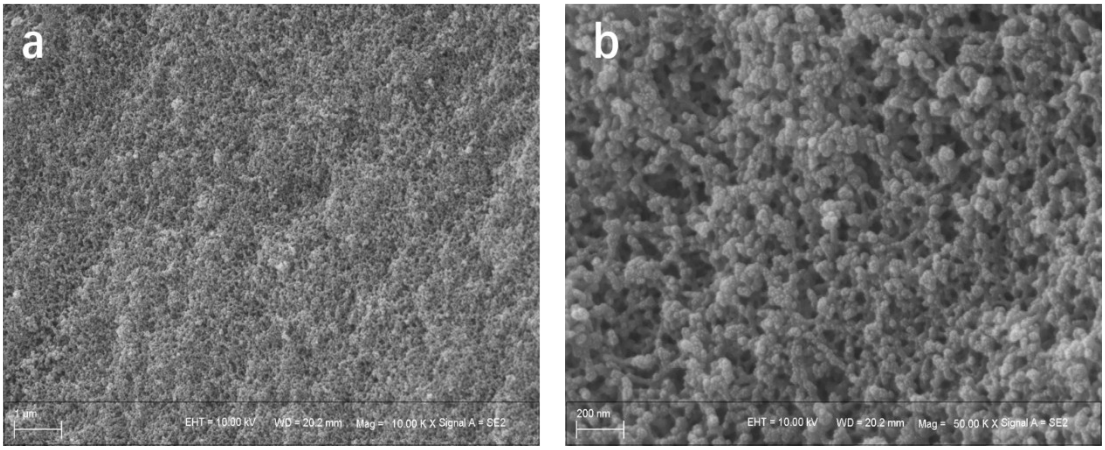

Figure S2. (a-b) SEM images of Zn-GMP.

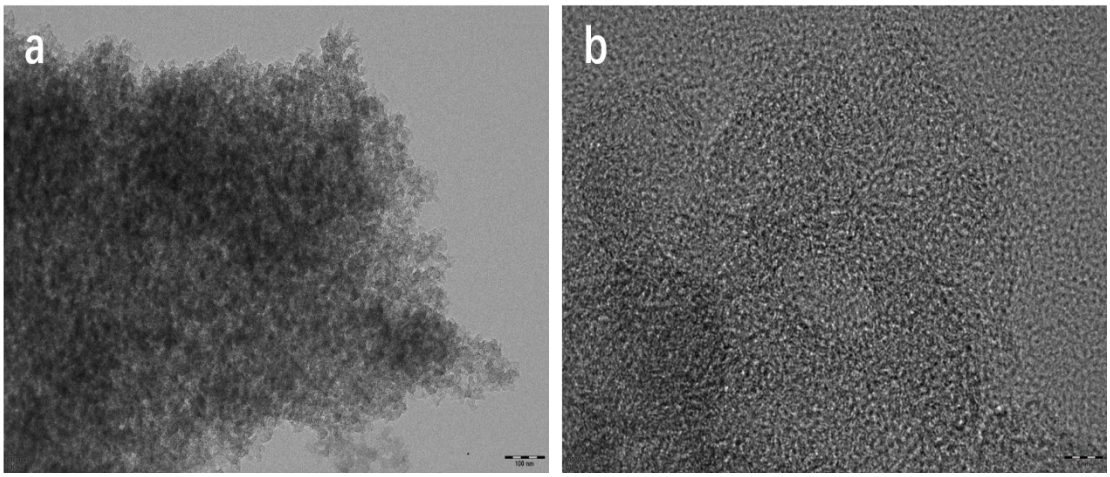

Figure S3. (a-b) TEM images of Zn-GMP.

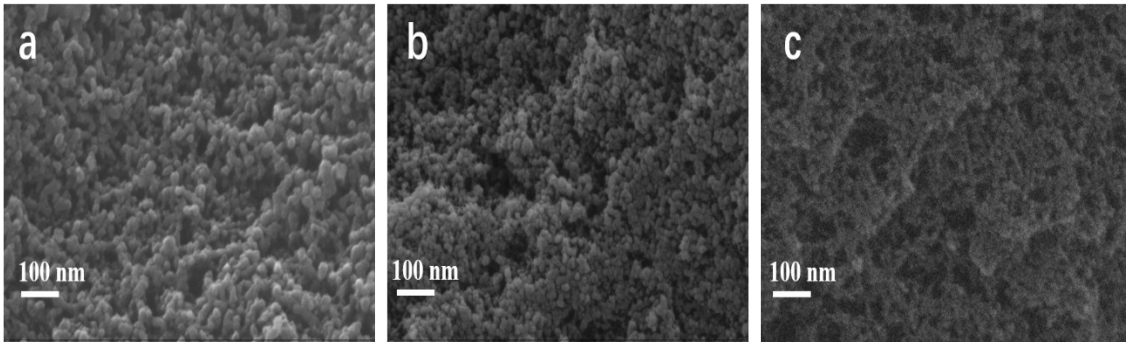

Figure S4. (a) SEM image of NP-HPCN-700. (b) SEM image of NP-HPCN-800. (c) SEM image of NP-HPCN-1000.

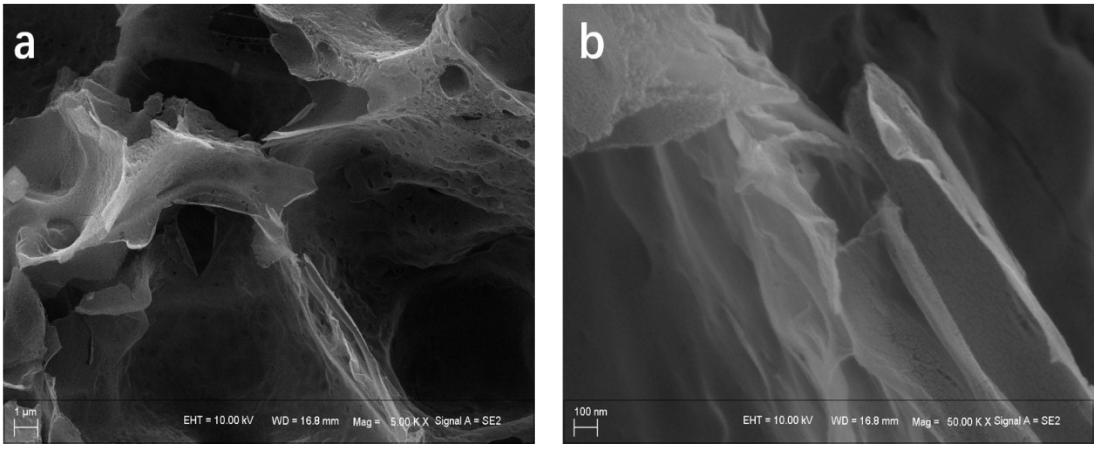

Figure S5. (a-b) SEM images of NP-HPC-900.

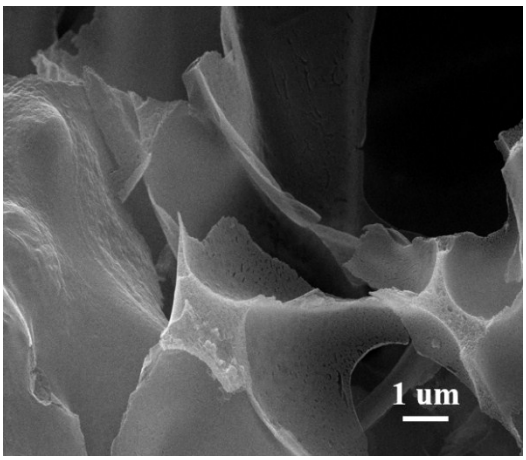

Figure S6. SEM image of carbons derived from the only GMP.

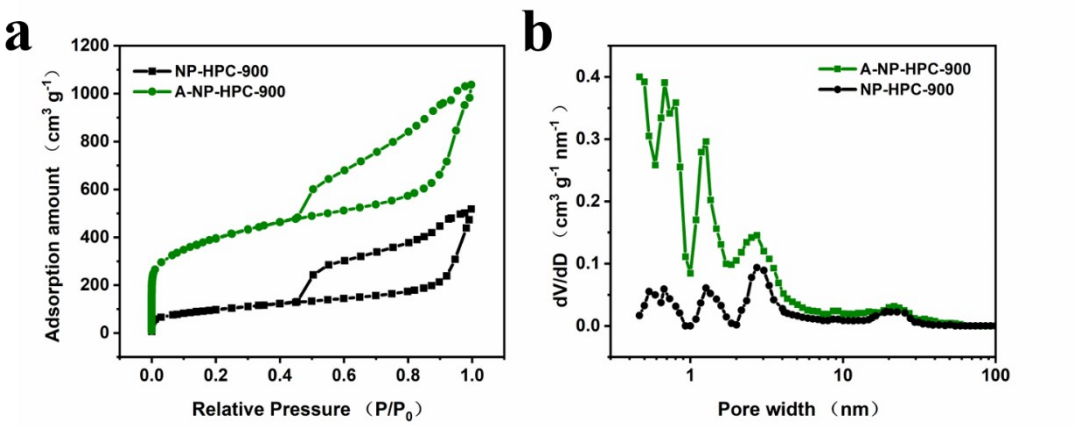

Figure S7. (a) N_2-adsorption/desorption isotherms. (b) the corresponding pore-size distribution curves calculated from the adsorption branch of the isotherms by: the NLDFT method.

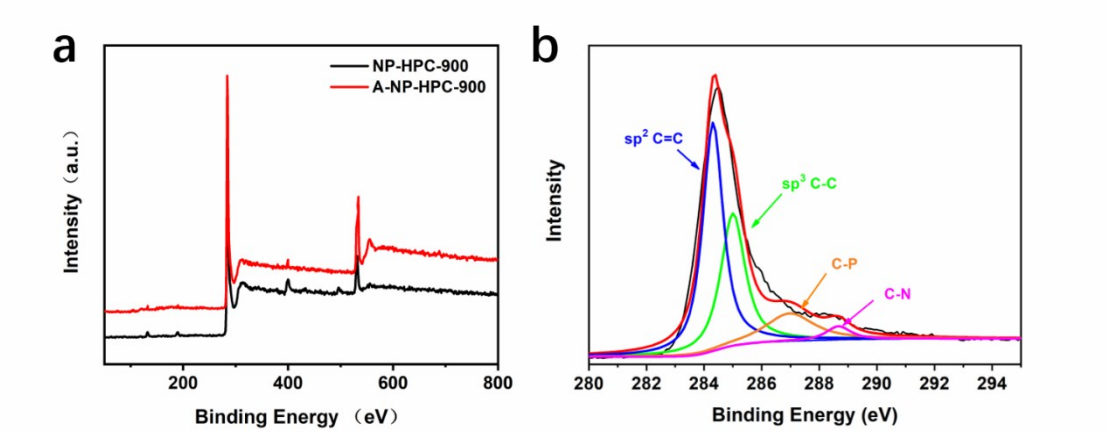

Figure S8. (a) Full-scale XPS spectra of NP-HPC-900 and A-NP-HPC-900. (b) high-resolution C 1s core-level XPS spectra of NP-HPCN-900.

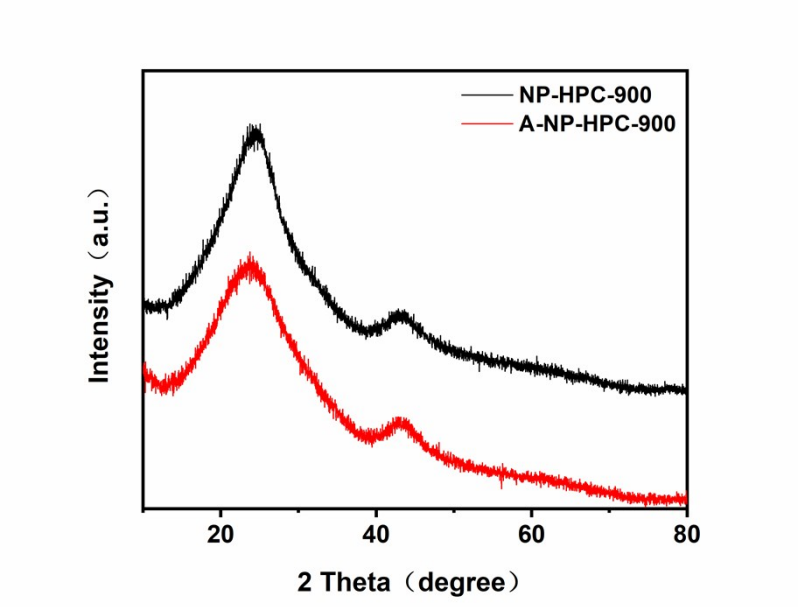

Figure S9. X-ray diffraction patterns of NP-HPC-900 and A-NP-HPC-900.

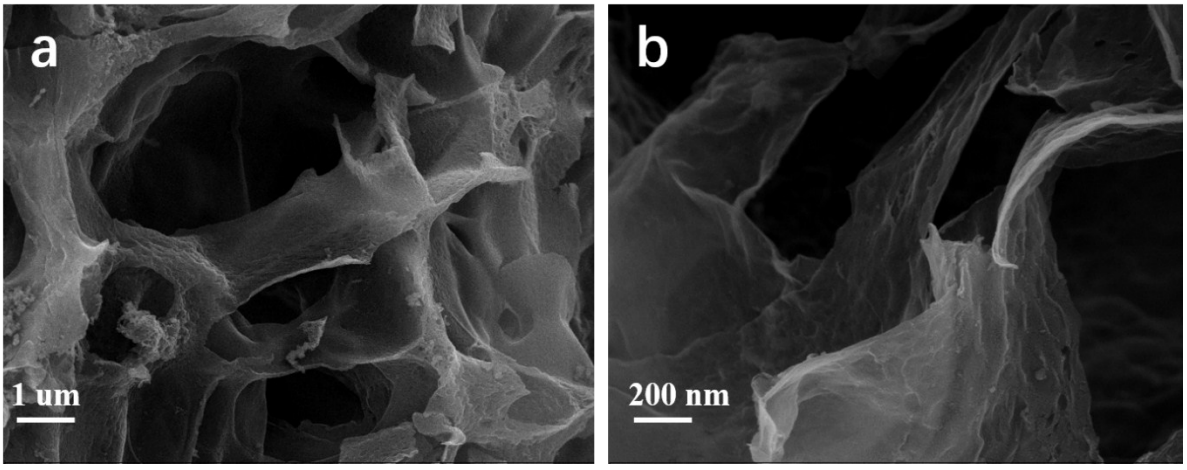

Figure S10. (a-b) SEM images of A-NP-HPC-900.

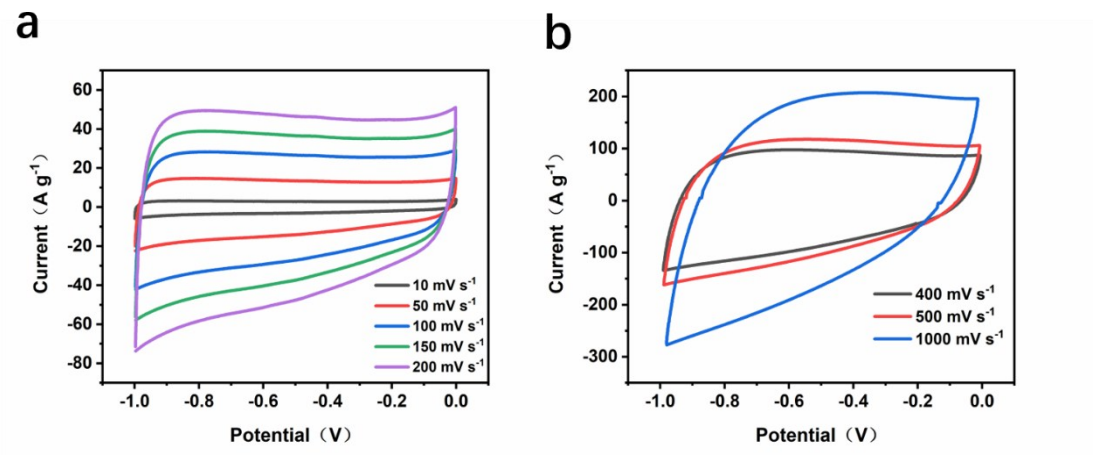

Figure S11. (a) CVs of NP-HPCN-900 electrode at a scan rate of 10-200 mV s^{-1}. (b) CVs of NP-HPCN-900 electrode at a scan rate of 400-1000 mV s^{-1}.

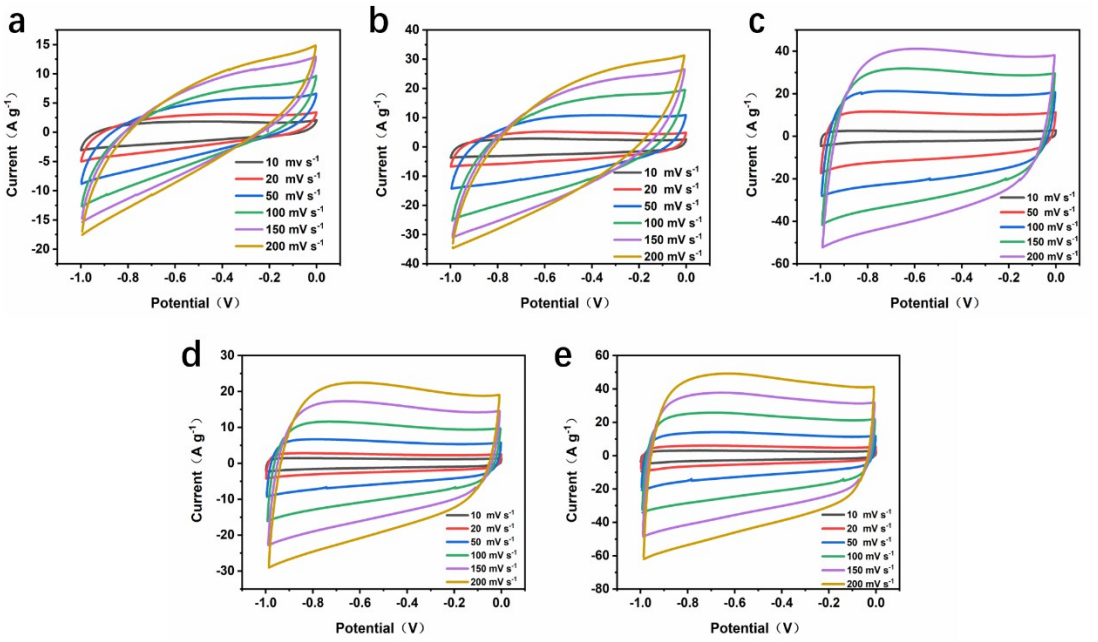

Figure S12. CVs at a scan rate of 10-200 mV s^{-1} (a) NP-HPCN-700. (b) NP-HPCN-800. (c) NP-HPCN-1000. (d) NP-HPC-900 and (e) A-NP-HPC-900.

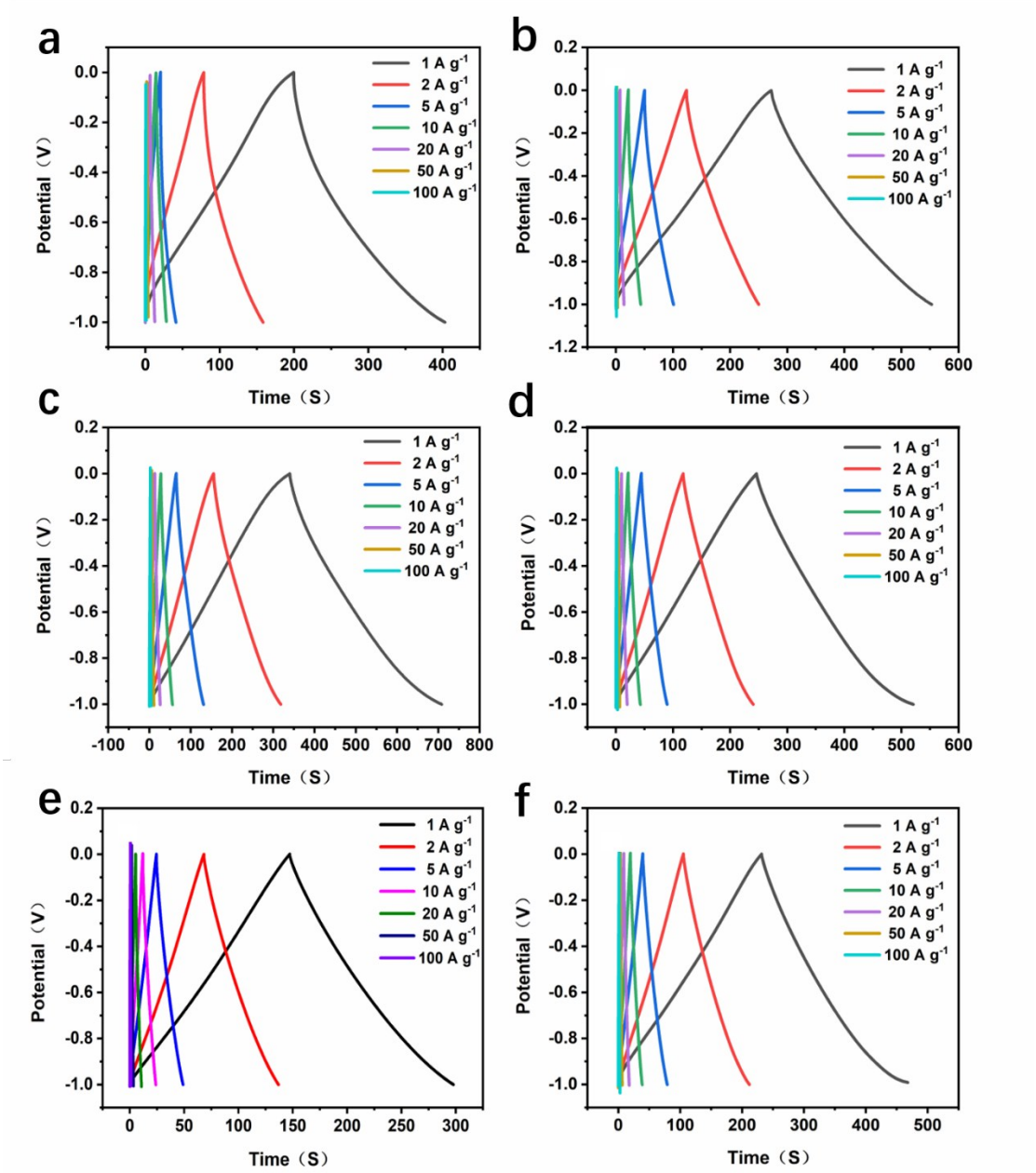

Figure S13. GCD curves at current densities of 1 to 100 A g^{-1} (a) NP-HPCN-700. (b) NP-HPCN-800. (c) NP-HPCN-900. (d) NP-HPCN-1000. (e) NP-HPC-900 and (f) A-NP-HPC-900.

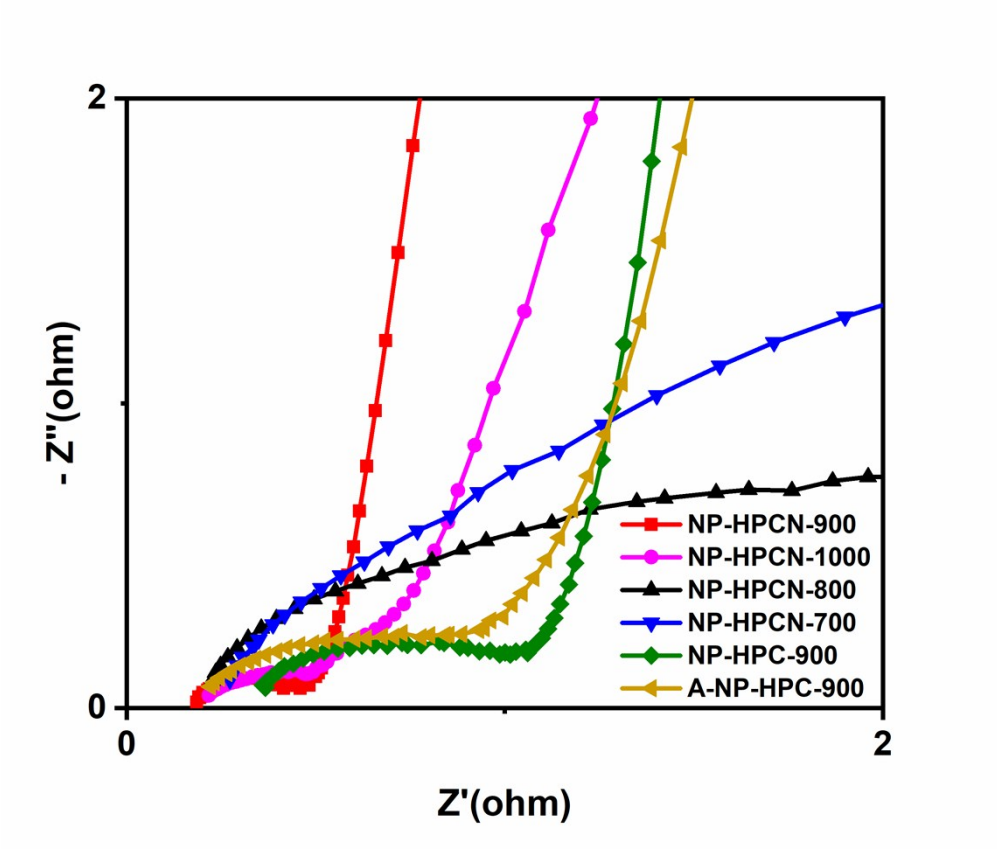

Figure S14. the Nyquist plots of the carbon specimens.

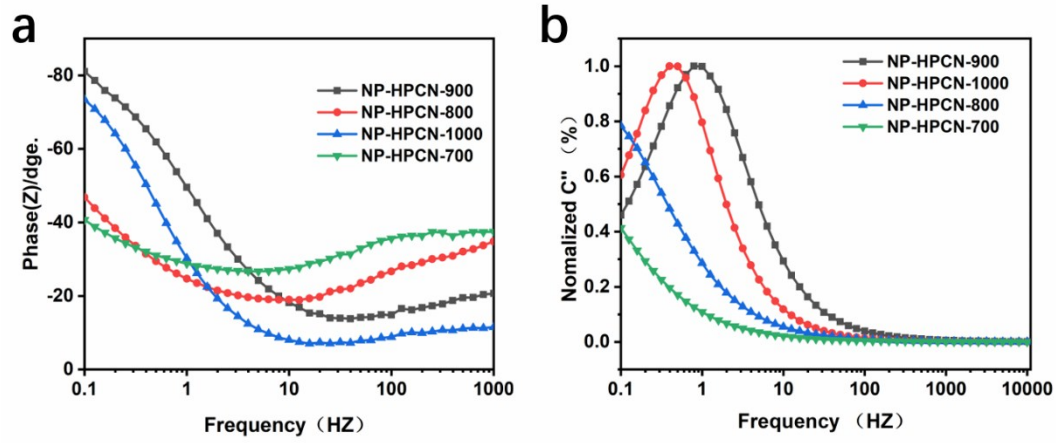

Figure S15. (a) the bode phase diagrams. (b) the normalized real and imaginary of carbon samples.

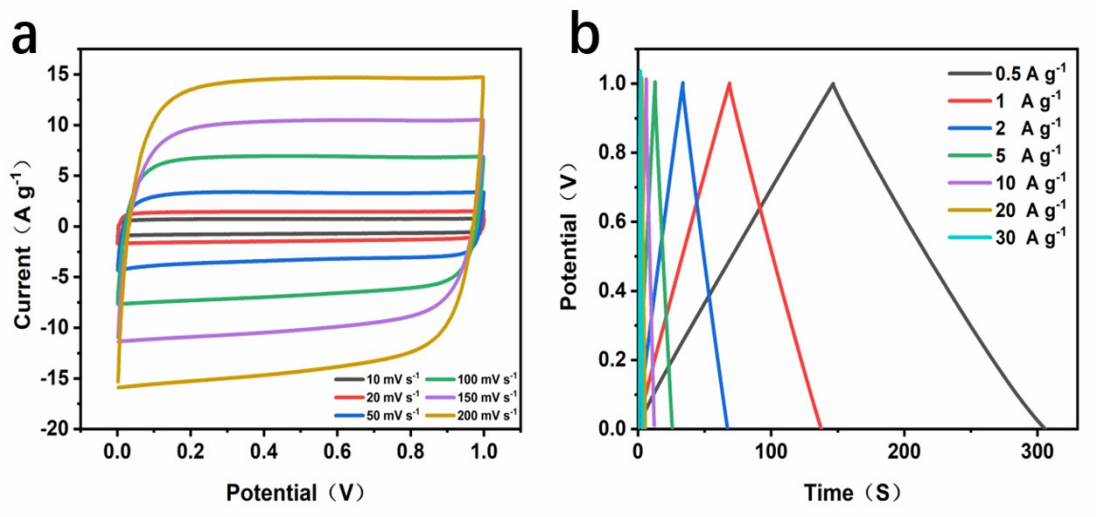

Figure S16. (a) CVs at a scan rate of 10-200 mV s^{-1} of NP-HPCN-900-KOH with a cell voltage of 0-1 V. (b) GCD curves at current densities of NP-HPCN-900-KOH with a cell voltage of 0-1 V.

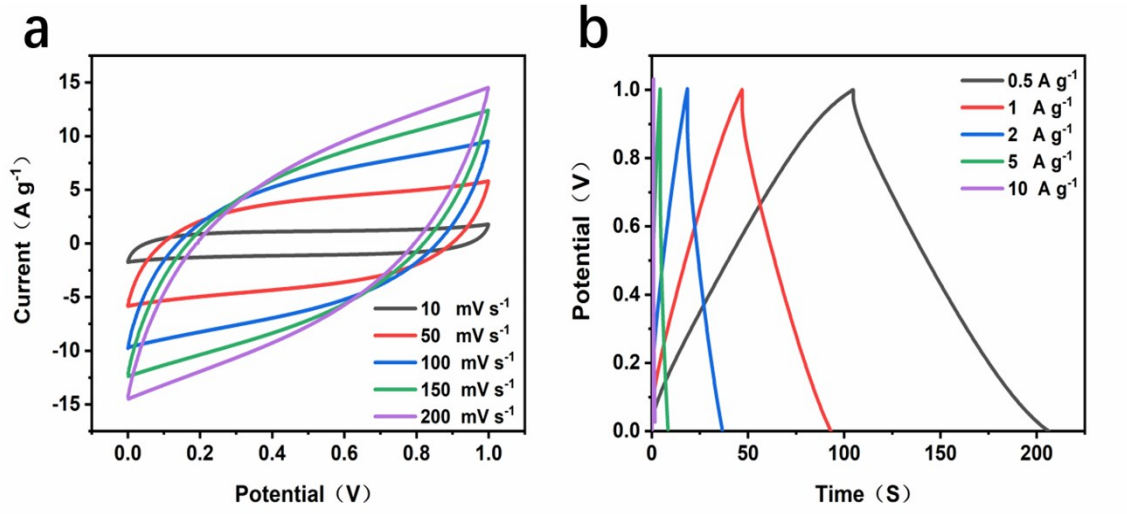

Figure S17. (a) CVs at a scan rate of 10-200 mV s^{-1} of NP-HPCN-900-PVA/KOH with a cell voltage of 0-1 V. (b) GCD curves at current densities of NP-HPCN-900-PVA/KOH with a cell voltage of 0-1 V.

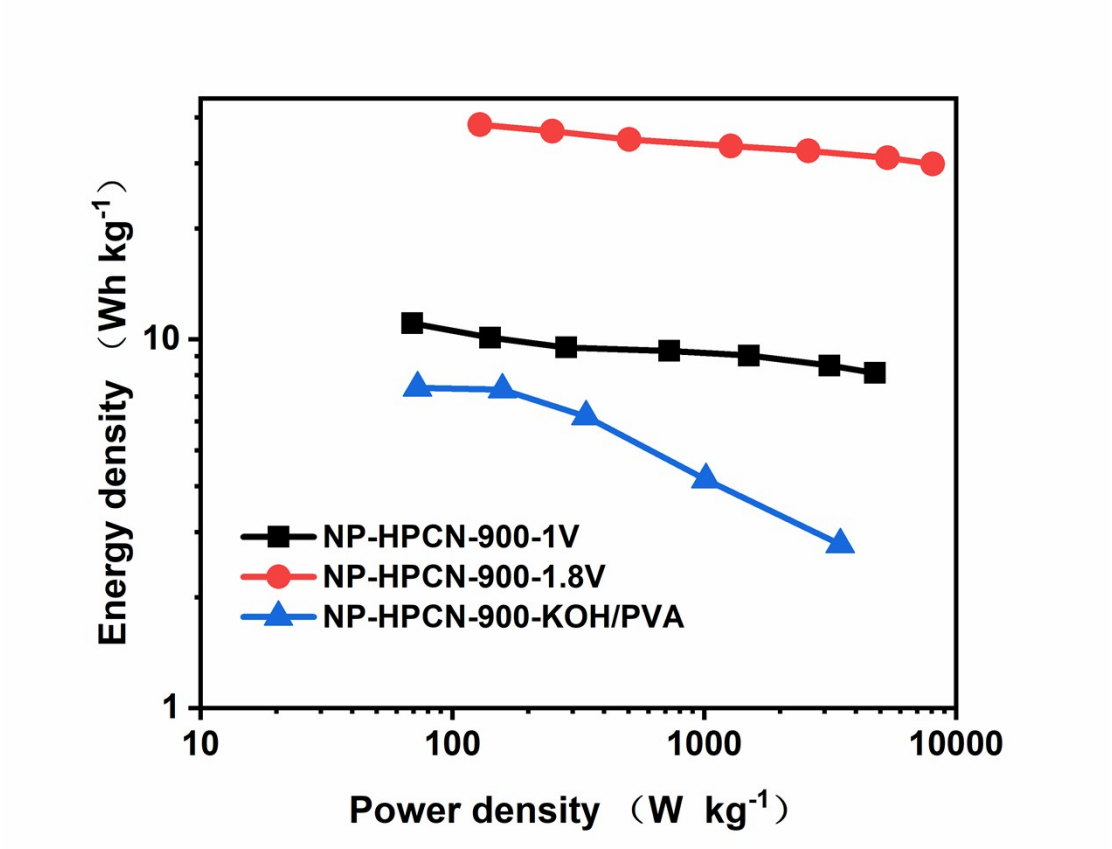

Figure S18. Ragone plot (energy density vs. power density) of the NP-HPCN-900 based symmetric device.

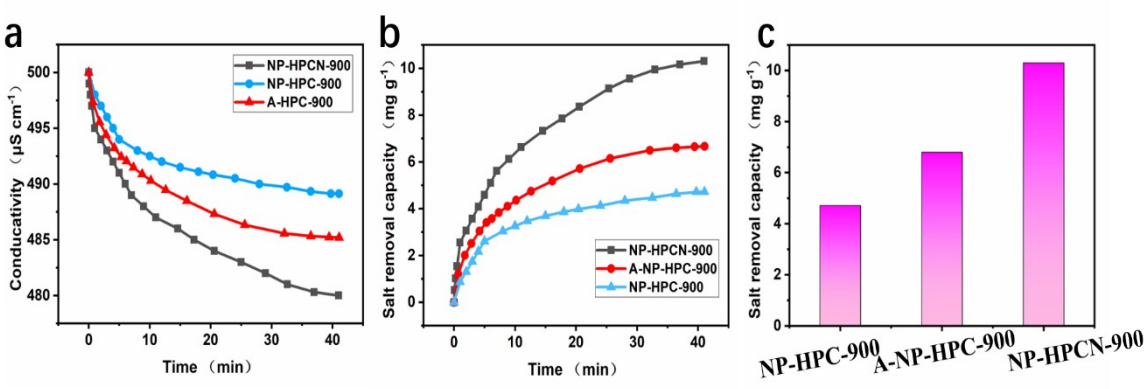

Figure S19. (a) Variation of solution conductivity vs. time. (b) The SAC curves. (c) The SAC histogram of NP-HPC-900, A-NP-HPC-900 and NP-HPCN-900.

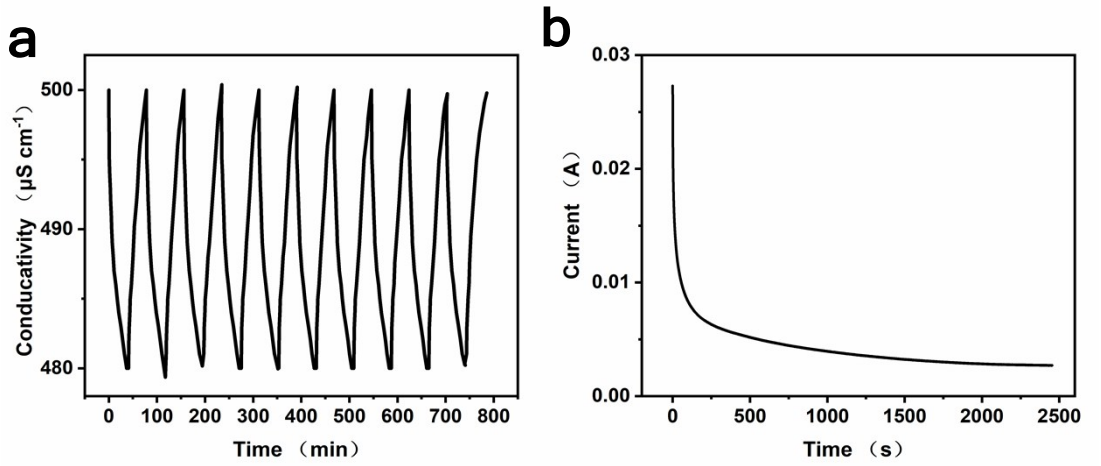

Figure S20. (a) Cycling stability of NP-HPCN-900 electrode. (b) Current response of NP-HPCN-900 electrode at 1.2 V.

Theoretical Calculations

The spin-polarized density functional theory (DFT) calculations were all performed by using the plane wave basis set based Vienna ab initio simulation package (VASP). Perdew-Burke-Ernzerhof (PBE) functional was adopted to describe the interaction between electrons and the cutoff energy of 400 eV was adopted for plane wave basis set. All the atoms were allowed to relax until the residue forces on each atom were less than 0.02 eV/Å. The graphene model used in our calculation consists of 12.30 × 29.83 × 15.00 $Å^3$. The vacuum region was set larger than 15 Å in z direction to prevent the interaction between two adjacent surfaces. A 3×1×1 Monkhorst-Pack sampled k-points in the irreducible Brillouin zone for structure optimization. All the configurations are built by Material studio (MS). The pyridinic-N doped single layer graphene was obtained by replacing the one carbon atom at the edge of the six-membered ring with nitrogen. And the N/P dual-doped single layer graphene was modelled by replacing the carbon atom connected between six-membered rings by phosphorus atom to form the P-C bond. These stable configurations are shown in Figure S18.

To evaluate the stability of Na and Cl adsorbed on graphene nanoribbons, we calculated the adsorption energy (Eads) of one Na^+ or Cl^- on the surface as follows,

$$E_{ads} = E_{tot} - E_{surf} - E_{NaorCl}$$

E_{tot} and E_{surf} are the total energies of graphene with and without potassium adsorption, $E_{Na\ or\ Cl}$ is the energy for single Na or Cl involved its bulk structures.

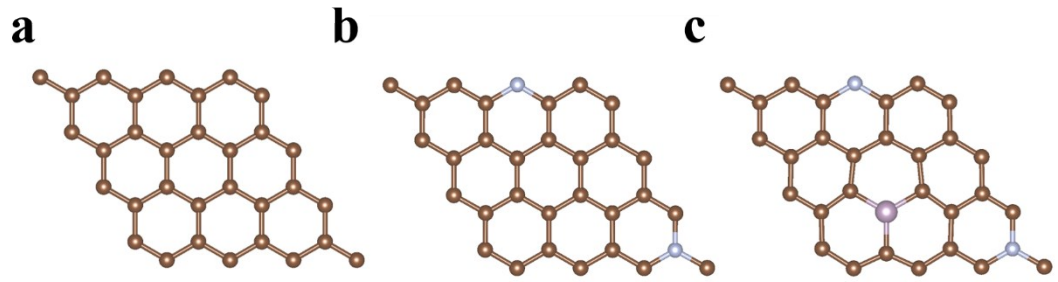

Figure S21. Top views of (a) single layer graphene. (b) N doped single layer graphene. (c) N/P dual-doped single layer graphene.

Table S1 BET surface area and pore structure parameters of NP-HPCNs, NP-HPC-900 and A-NP-HPC-900 samples.

Samples	[a] S_{BET} ($m^2 g^{-1}$)	[b] S_{micro} ($m^2 g^{-1}$)	[c] S_{meso} ($m^2 g^{-1}$)	[d] S_{macro} ($m^2 g^{-1}$)	[e] Mean pore diameter（nm）	[f] V_t ($cm^3 g^{-1}$)	[g] V_{micro} ($cm^3 g^{-1}$)	[h] V_{meso} ($cm^3 g^{-1}$)	[i] V_{macro} ($cm^3 g^{-1}$)
NP-HPCN-1000	1310	849	434	27	4.46	1.46	0.39	0.92	0.15
NP-HPCN-900	1679	1053	587	39	4.31	1.81	0.46	1.13	0.22
NP-HPCN-800	763	544	205	14	3.30	0.63	0.23	0.32	0.09
NP-HPCN-700	553	454	94	5	2.68	0.37	0.19	0.15	0.03
NP-HPC-900	402	103	280	19	6.77	0.68	0.05	0.52	0.11
A-NP-HPC-900	1541	1056	454	31	4.05	1.56	0.47	0.93	0.16

[a] Surface area calculated based on adsorption isotherms; [b] t-plot micropore volume; [c] S_{meso} calculated from BJH adsorption cumulative surface area; [d] S_{macro} was acquired by subtracting S_{micro} and S_{meso} from S_{BET}; [e] 4V/A by BET; [f] total pore volume at p/p0 = 0.995; [g] t-plot micropore volume; [h] BJH adsorption cumulative volume; [i] V_{macro} was acquired by subtracting V_{micro} and V_{meso} from V_t.

Table S2 Chemical compositions of as-prepared samples calculated from XPS results.

Samples	at.% C	at.% O	at.% N	at.% P
NP-HPCN-700	71.78	16.50	9.41	2.31
NP-HPCN-800	74.34	14.76	8.55	2.35
NP-HPCN-900	87.01	7.55	4.20	1.24
NP-HPCN-1000	92.07	5.04	2.10	0.79
NP-HPC-900	88.66	6.32	3.82	1.20

Table S3 comparison of salt adsorption capacity between NP-HPCN-900 and previous literatures.

Sample	Voltage (V)	Initial Concentration (mg/L)	Salt adsorption capacity (mg/g)	Ref.
3D Channel-structured graphene	1.5	295	9.60	1
Carbon spheres with hierarchical micro/mesopores	1.2	500	15.8	2
Porous carbon polyhedra	1.2	500	13.8	3
Porous carbon spheres	1.2	500	5.81	4
GN/hierarchically porous carbon	1.2	500	6.18	5
CHS1	1.6	250	18.8	6
Biomass-derived porous carbon	1.5	500	16	7
Nafion-AC	1.2	500	10.8	8
NP-HPCN-900	1.2	250	10.3	This work
NP-HPCN-900	1.4	250	18.1	This work

Reference:

1 L. Chang, Y. H. Hu, *J. Colloid Interface Sci*., 2019, **538**, 420-425.
2 X. Xu, H. Tang, M. Wang, Y. Liu, J. Mater. Chem. A, 2016, 4, 16094-16100.
3 Y. Liu, X. Xu, M. Wang, T. Lu, Z. Sun, L. Pan, Chem Commun., 2015, 51, 12020-12023.
4 Y. Liu, L. Pan, T. Chen, X. Xu, T. Lu, Z. Sun, D. H. C. Chua, Electrochimica Acta, 2015, 151, 489-496.
5 X. Wen, D. Zhang, T. Yan, J. Zhang and L. Shi, J. Mater. Chem. A, 2013, 1, 12334-12344.
6 Z. Y. Leong, H. Y. Yang, RSC Advances, 2016, 6, 53542-53549.
7 Z. Xie, X. Shang, J. Yan, T. Hussain, P. Nie, J. Liu, *Electrochim. Acta*, 2018, **290**, 666-675.
8 W. Cai, J. Yan, T. Hussin, J. Liu, *Electrochim. Acta*, 2017, **225**, 407-415.